Submitted to the Astrophysical Journal
Preprint typeset using LaTeX style emulateapj v. 5/2/11

A SYSTEMATIC RETRIEVAL ANALYSIS OF SECONDARY ECLIPSE SPECTRA II: A UNIFORM ANALYSIS OF EIGHT PLANETS AND THEIR C TO O RATIOS

Michael R. Line, Heather Knutson, Aaron S. Wolf, and Yuk L. Yung
Division of Geological and Planetary Sciences, California Institute of Technology, Pasadena, CA 91125
Submitted to the Astrophysical Journal

ABSTRACT

Secondary eclipse spectroscopy provides invaluable insights into the temperatures and compositions of exoplanetary atmospheres. We carry out a systematic temperature and abundance retrieval analysis of eight exoplanets (HD189733b, HD149026b, GJ436b, WASP-12b, WASP-19b, WASP-43b, TrES-2b, and TrES-3b) observed in secondary eclipse using a combination of space- and ground-based facilities. Our goal with this analysis is to provide a consistent set of temperatures and compositions from which self-consistent models can be compared and to probe the underlying processes that shape these atmospheres. This paper is the second in a three part series of papers exploring the retrievability of temperatures and abundances from secondary eclipse spectra and the implications of these results for the chemistry of exoplanet atmospheres. In this investigation we present a catalogue of temperatures and abundances for H_2O, CH_4, CO, and CO_2. We find that our temperatures and abundances are generally consistent with those of previous studies, although we do not find any convincing evidence for super-solar C to O ratios in any of the planets analyzed here. Furthermore, within our sample we find little evidence for thermal inversions over a wide range of effective temperatures, consistent with previous investigations. The lack of evidence for inversions over such a wide range of effective temperatures provides additional support for the hypothesis that TiO is unlikely to be the absorber responsible for the formation of these inversions.

1. INTRODUCTION

There are currently more than fiffty extrasolar planets with published secondary eclipse measurements (e.g., Knutson et al. 2010), with many more observations taken but not yet published. These data come from both space and ground-based facilities, and span wavelengths ranging from the visible to the mid-infrared. The combination of data from multiple telescopes spanning a broad range of wavelengths offers an invaluable tool for constraining the pressure-temperature profiles and compositions of exoplanetary atmospheres. With an increasingly larger sample of spectra, we can begin to understand the underlying physical and chemical processes that control the atmospheric abundances through comparative exoplanetology.

There are several interesting questions that we might address through a comparative study of exoplanet atmospheres. One is the frequency of planets with super-solar C to O ratios. The C to O ratio can potentially provide constraints on the region of the disk where the planet formed (Öberg, Murray-Clay, & Bergin 2011; Madhusudhan et al. 2011b). These studies propose that planets that accrete their gas envelopes outside of the water snow line will have modestly super-solar C to O ratios, which increase to even higher values for planets that form beyond the CO_2 ice line (Öberg, Murray-Clay, & Bergin 2011).

A uniform analysis of hot Jupiter atmospheres can also be used to investigate the origin of the temperature inversions detected in a subset of these planets. It has been suggested (Hubeny et al. 2003; Fortney et al. 2008) that gas-phase TiO and VO, which are effective absorbers at optical wavelengths, could lead to the formation of temperature inversions in these atmospheres. TiO and VO thermochemically exist in the gas phase in hotter planets ($T_{eq} > 2000$ K). Therefore, one would expect thermal inversions to be limited to planets that are hot enough to have gas phase TiO in their upper atmospheres. However, in a more recent study Spiegel et al. (2009) suggested that vigorous vertical mixing is required to keep both gas phase and condensed phase TiO and VO aloft in upper, inversion forming regions of the atmosphere. Showman et al. (2009) demonstrated that TiO could be severely depleted due to cold traps in the deep atmosphere and on the planet's night side. Furthermore, should TiO and VO persist despite the aforementioned reasons, Knutson et al. (2010) speculated that high amounts of UV flux from active stars might dissociate TiO and VO. Recently Madhusudhan (2012) proposed that the abundances of TiO and VO could be significantly depleted if the atmosphere has a super-solar C to O ratio. In this paper we use a uniform retrieval analysis to determine if there is a correlation between the presence or absence of a temperature inversion, the C to O ratio of the planet's atmosphere, and the activity level of its host star.

In Paper I (Line et al. 2013) we developed a suite of inverse modeling algorithms, called CHIMERA, to determine the ranges of temperatures and compositions that were consistent with a given data set. CHIMERA uses three Bayesian retrieval approaches including optimal estimation, bootstrap Monte Carlo, and differential evolution Markov chain Monte Carlo to determine the allowable ranges of temperatures and abundances for a given planet. In this investigation we apply CHIMERA to eight planets in order to undertake the first uniform retrieval analysis of a set of exoplanet spectra. Our uniform

mrl@gps.caltech.edu
[1] Correspondence to be directed to mrl@gps.caltech.edu

analysis allows us to make robust comparisons between planets, as we utilize the same model parameters and retrieval techniques for each target. Comparing results derived from different retrieval approaches or different models can be complicated due to the differing model assumptions. Such an analysis can also provide a useful set of statistical atmospheric properties from which detailed physical models such as general circulation models, photochemical models, and radiative equilibrium models can be compared.

Our goal in this study is to provide a catalogue of temperatures and abundances for eight well-observed planets and to address some of the outstanding questions regarding C to O ratios and the possible causes of thermal inversions. Our sample includes the following planets: HD189733b, GJ436b, HD149026b, WASP-12b, WASP-19b, WASP-43b, TrES-2b, and TrES-3b. These planets were selected because they span a wide range of physical parameters with a reasonably high number of spectral data points per planet. In §2 we will describe the retrieval approaches and forward model assumptions. The details of our approach can be found in Paper I. In §3 we present our temperature and abundance retrieval results for each of the eight planets and compare them to previously published analyses. We then use the derived abundances to asses the allowed range of C to O ratios and comment on the implications of these results for current hypotheses for the origin of temperature inversions on these planets. Finally, in §4 we will discuss the big picture view from our retrieval results, which show little evidence for C to O ratios larger than one.

2. METHODS

We summarize our retrieval methods and forward models here and refer the reader to Paper I for more detailed descriptions. The goal of a retrieval, given some forward model, is to characterize the posterior probability distribution of the parameters of interest, in this case, temperatures and abundances via a radiative transfer model. This posterior is determined from a combination of prior information and the data. Paper I describes three approaches that are commonly used to characterize posterior distributions. These include: optimal estimation (OE, e.g., Rodgers 2000), bootstrap Monte Carlo (BMC, Press 1992; Ford 2005), and differential evolution Markov chain Monte Carlo (DEMC, ter Braak 2006). Optimal estimation minimizes a quadratic cost function using the Levenbergh-Markquardtt scheme and approximates the posterior as multivariate normal. Bootstrap Monte Carlo uses a data resampling method based on a best model fit to derive the parameter distributions. Differential evolution Markov chain Monte Carlo is a type of Markov Chain Monte Carlo approach (MCMC) which uses a genetic algorithm to efficiently explore highly correlated parameter spaces. DEMC and OE both evaluate the following log-likliehood function:

$$\chi^2(\mathbf{x}) = (\mathbf{y} - \mathbf{F}(\mathbf{x}))^T \mathbf{S_e^{-1}} (\mathbf{y} - \mathbf{F}(\mathbf{x})) + (\mathbf{x} - \mathbf{x_a})^T \mathbf{S_a^{-1}} (\mathbf{x} - \mathbf{x_a}) \quad (1)$$

where $\mathbf{y}$ is the set of n data points, $\mathbf{x}$ is the m-dimensional parameter vector, $\mathbf{F}(\mathbf{x})$ is the forward model, and $\mathbf{S_e}$ is the $n \times n$ data error matrix. $\mathbf{x_a}$ is the *a priori* state vector and $\mathbf{S_a}$ is the $m \times m$ *a priori* covariance matrix. The first term in equation 1 is simply the standard "chi-squared" and the second term represents the prior knowledge of the parameter distribution before we make the observations.

In Paper I we determined that the three approaches agree for high signal-to-noise, high-resolution data, but diverge for the data sets currently available for typical hot Jupiters. We also found that OE and DEMC tended to agree better than the BMC, and that our implementation of BMC was only able to characterize the probability distribution in the region very close to the nominal solution. Therefore, in this investigation we utilize the OE and DEMC approaches to estimate the posterior probability distributions of the temperatures and abundances. We use the results from OE to initialize the DEMC as described in Paper I. By using two distinct approaches, we can determine whether or not our results are sensitive to our choice of fitting method. We present results from the DEMC approach in our final abundance catalogue, as this is the more widely accepted, robust approach for current exoplanet data (e.g, Benneke & Seager 2012; Line et al. 2013).

The physical parameters we are most interested in are the temperature structure and the mole fractions of various gases. We therefore choose to retrieve constant-with-altitude mixing ratios of H_2O, CH_4, CO, and CO_2. These are generally the most thermochemically abundant (with the exception of CO_2) and infrared active species over the observational bandpasses for a variety of metallicities and C/O ratios. Furthermore these species tend to have the most complete line lists (see Part I for description of our line lists). We have assumed constant-with-altitude because the data do not provide useful constraints on the vertical abundance profile (Lee et al. 2012). Also, the species of interest in this case, when abundant, thermochemically have near constant-with-altitude profiles to begin with, and vertical mixing tends to quench minor species resulting in constant-with-altitude profiles (Moses et al. 2011; Line et al. 2011). We note that we have not included other potentially important absorbers such as NH_3, HCN, H_2S, C_2H_2, as accurate line-lists at high temperatures do not yet exist (to the best of our knowledge). We plan to expand the scope of our future retrievals as more reliable sepctroscopic databases become available.

We also assume that these planets are hydrogen dominated and hence fix the H_2 and He mixing ratios to thermochemically appropriate abundances of 0.85 and 0.15, respectively, which hold over a wide range of temperatures and metallicities. There could also be other optically inactive species such as N_2, O_2 , noble gases other than He, etc., but these molecules would have a minimal impact on the shape of our retrieved emission spectra and we therefore do not include them in our fits. The retrievable species are assumed to have mole fractions much much less than that of H_2, therefore we do not include mean molecular weight effects on the spectrum.

In Paper I we described two temperature retrieval approaches: the level-by-level approach and the parametrized approach. For this analysis we choose to use the parametrized temperature profile approach. The limited number of data points per planet limits the practicality of a full level-by-level retrieval. The parameterization we use is based on analytic radiative equilibrium

profiles (see Guillot 2010; Heng et al. 2012; Robinson & Catling 2012) controlled by 5 free parameters. These parameters are the infrared opacity, two visible opacities, partitioning of the two opacity streams, and a catch-all factor for the albedo, emissivity, and redistribution. This last parameter effectively accounts for energy balance at the top of the atmosphere. We do not try to self-consistently relate the temperatures back to the composition for reasons discussed in Paper I. Once we have determine the uncertainty distributions for each of the five temperature profile parameters, we can then reconstruct the ensemble of temperature profiles.

Our priors are the same as those described in Paper I. When using the optimal estimation formalism, by construction, the priors are Gaussian. We choose very broad (12 orders-of-magnitude spanning the 68% confidence interval) gas priors. This mitigates the effect of the prior on the gas abundance retrievals. We also choose broad Gaussian priors on the 5 parameters govern the parametrized temperature profile. When using DEMC we choose flat gas priors, but use Gaussian priors on the temperature parameters. These produce a spread in the reconstructed temperature profiles that is more consistent with numerical radiative equilibrium models than a flat prior would. For any MCMC search when using flat priors one must impose limits in order to prevent the random walk process from venturing too far from useful phase space. We choose a lower limit mixing ratio of 10^{-12} and an upper limit of 0.1. Although somewhat arbitrary, we would expect the molecular abundances of these four species to fall well within these limits.

We obtain the planet and system parameters (stellar radius, planet radius, stellar temperature, semimajor axis, planet gravity) from the published literature (see Table 1). These parameters are used in generating the parameterized temperature profile and when dividing by the stellar grid models. We use interpolated (logg, Fe/H, and Teff) PHOENIX stellar grid models (Allard et al. 2000) to compute the contrast spectrum.

3. RETRIEVAL ANALYSIS

In this section we provide a catalogue of abundances and temperatures for eight planets observed in secondary eclipse. The sources of the secondary eclipse data are shown in Table 2. We provide detailed descriptions of the results for each planet in our sample and compare these results to those of previous investigations. Graphical results of the retrievals are summarized in Figures 1-3. Figure 1 shows the secondary eclipse observations, the best fit spectra, and a statistical summary of all of the fits from the DEMC retrieval. These fits are summarized with 68% and 95% confidence bounds along with a median spectrum. Figure 2 shows the temperature profiles summarized with 68% and 95% confidence bounds, a median profile, and a best fit. We also show the averaged thermal emission contribution function to get a sense for which pressure levels the observations probe. Finally, Figure 3 shows the marginalized gas abundance posteriors for each planet along with the imposed priors (flat for DEMC, Gaussian for OE). We use the resulting retrieval results to derive the C to O ratio probability distributions in Figure 4. These distributions generally have a double-peaked structure, which is the manifestation of the uniform abundance priors in the C to O distribution (see Paper I for a detailed discussion of this issue). Rather than showing the two peaked C to O distribution resulting from the prior and posterior together, we normalize the posterior derived C/O distribution by the double-peaked prior C/O distribution to give us a sense for how the data contributed to our knowledge of the C to O ratio. This is not a statistically rigourous approach, but it provides a clear visual representation of the information provided by the observations independent of the assumed priors.

We also include a Table (Table 3) comparing our numerical results to those of previous studies for easy reference. We provide our 68% confidence intervals for the molecular mixing ratios along with the nominal best-fit values derived from DEMC. We also report the reduced cost function value from equation 1, χ^2/N for the best fit, where N is the number of data points. A $\chi^2/N$of one suggests that the model on average fits the data within the 1-sigma error bars (just as in Madhusudhan & Seager 2009). Since we place limits on the flat gas priors used in the DEMC retrieval, we must interpret the retrieved abundance range in the context of those limits. Given those limits, the 68% confidence interval from the flat gas prior would result in abundances that span $8.15 \times 10^{-11} - 1.51 \times 10^{-2}$, or ∼8 orders of magnitude. Anything smaller than this suggests that the data was informative within the context of our model. Furthermore, we quote the 68% confidence interval for the C/O ratios derived from our abundance retrievals. These values are computed directly from the posterior C to O distributions, not the normalized-by-prior distribution shown in Figure 4. Given the imposed abundance limits, the 68% confidence interval in the C/O distribution resulting from the uniform gas priors is $5.10 \times 10^{-2} - 1.45 \times 10^{1}$, or ∼ 3 orders of magnitude.

3.1. *HD189733b*

Together with HD209458b, HD189733b is one of the best-studied hot Jupiters to date. This is because it orbits a bright, nearby K star with a favorable planet-star radius ratio. Secondary eclipse observations have been made with a variety of instruments including HST-NICMOS (Swain et al. 2009), Spitzer IRAC (Charbonneau et al. 2008; Knutson et al. 2009; 2012; Agol et al. 2012), MIPS (Knutson et al. 2009; Charbonneau et al. 2008), and IRS (Grillmair et al. 2007; 2008) spanning ∼1.5 μm to ∼25 μm. Several previous retrieval investigations have constrained the range of allowable temperature structures and compositions for this atmosphere. The first complete study via a systematic parametric grid search was published by Madhusudhan & Seager (2009). The composition they derived was high (relative to a solar composition atmosphere) in CO_2 and CO followed by low abundances of CH_4 and a moderate abundance of H_2O. Lee et al. (2012) and Line et al. (2012) came to similar conclusions using the optimal estimation retrieval approach. The large abundance of CO_2 relative to the other species remains chemically perplexing (Line et al. 2010; Moses et al. 2011; 2013a). There is also no evidence for a thermal inversion.

Our abundances are generally consistent with the previous results to within an order of magnitude. However, not all of the previous investigations are consistent. For

instance, all of the results for HD189733b in Table 3, including ours, require an anomalously high abundance of CO_2 aside from the analysis presented in Swain et al. (2009) (see Shabram et al. (2011) for a more detailed discussion of this discrepancy). Also, the upper limit on CH_4 quoted by Line et al. (2012) is much higher than the limits from previous studies. This is likely due to the problems associated with using optimal estimation in data regimes in which the resulting posterior probability distributions are non-Gaussian. We note that the data used in the retrievals were not the same in all cases. We simultaneously retrieved the abundances and temperatures using a combination of data including the NICMOS, IRS, and Spitzer photometry. Madhusudhan & Seager (2009) considered these data sets separately. Swain et al. (2009) and Line et al. (2012) only considered the NICMOS data set. Lee et al. (2012) considered all available data sets. It is worth considering whether individual data sets give consistent results, as data taken at different epochs could vary as a result of stellar variability, differences in detector systematics, etc. Despite these differences the results of all of these studies are in generally good agreement, suggesting that our conclusions for this planet are reasonably robust.

In our new study we find an enhanced best fit C/O ratio of 0.85 (0.47-0.90), well within the range quoted by previous investigations. This is a fairly robust result relative to the prior (see Figure 4).

The large number of Spitzer IRS data points that have thermal emission weighting functions near the 10 mbar level combined with our requirement of radiative equilibrium via the analytic parameterization, provide a well constrained temperature profile above the 0.1 bar level. Below this level the temperature profile begins to diverge because very little emission is able to escape from these deeper regions of the atmosphere. Our derived spread in profiles in the well-constrained regime between 10-100 mbar is in agreement with the profile derived in Lee et al. (2012).

3.2. *GJ436b*

GJ436b is a warm (∼700-900 K) Neptune-mass planet with a seemingly unusual atmosphere chemistry that has generated considerable attention in the modeling community. The first set of Spitzer observations (Stevenson et al. 2010) indicated that this planet is rich in CO and depleted in CH_4. This conclusion is primarily driven by the high 3.6 to 4.5 μm flux ratio. This composition is at odds with its temperature given the assumption of thermochemical equilibrium and solar elemental abundances. One would expect such a planet to be rich in methane and low in CO. These authors suggested that photochemistry might be responsible for the apparent depletion of methane. However, photochemical depletion of methane does not appear to be significant in hydrogen dominated atmospheres in this temperature range even under a wide variety of assumed vertical mixing strengths and UV fluxes (Line et al. 2011; Miller-Ricci et al. 2012; Moses et al. 2013b). It has recently been suggested that this planet has an extremely metal-rich (300-2000× solar) atmosphere, which provides a simple explanation for the measured enhancement of CO over CH_4 without the need to invoke extreme or exotic chemistry (Moses et al. 2013b).

Table 3 shows how our results compare to those of Stevenson et al. (2011) and Madhusudhan & Seager (2011). We also conclude that the atmosphere is rich in CO and depleted in CH_4 relative to what one would expect for a solar composition atmosphere at these temperatures. We point out that although we quote a confidence interval, on all four gases, our fits only provide upper limits on most species with the exception of CO. Our lower limit for these unconstrained gases comes from our prior, which artificially places a hard limit at 1×10^{-12}. If we examine the histogram for methane in Figure 3 we see that an appropriate upper limit might be placed at the half max location of $\sim 10^{-7}$, which is within an order of magnitude of the previous results. We also find upper limits on the CO_2 and H_2O abundances, but again no strong lower limit. The CO_2 marginalized posterior shows a multimodal behavior, with a strong mode occurring at $\sim 10^{-7}$ and a weaker mode near $\sim 10^{-3}$. Our estimate of the C to O ratio is similar to that quoted by Madhusudhan & Seager (2011) as the most probable values seem to fall between solar and unity. Figure 4 indicates that a C to O ratio greater than one is highly improbable. Our temperature profile dispersion is nearly identical to those found in Madhusudhan & Seager 2011 between ∼0.1-1 bars.

3.3. *HD149026b*

To date there has been no detailed atmospheric retrieval analysis for this planet. It is a Saturn-mass planet with a very large core orbiting a metal-rich star (Sato et al. 2005), and therefore is a good candidate for a metal-rich atmosphere. Furthermore, its likely high atmospheric metallicity and temperature make it a prime candidate for an inversion caused by gas-phase TiO and VO (Fortney et al. 2006). Stevenson et al. (2012) obtained Spitzer photometry and interpreted the observations using the self-consistent models from Fortney et al. (2005; 2006; 2008). These data-model comparisons suggest that the planet's emission spectrum is well-described by a relatively high (30× solar) metallicity atmosphere with correspondingly enhanced CO and CO_2 features, with no evidence for a temperature inversion.

Our retrieval results indicate that the planet has more CO and CO_2 than methane, consistent with the Stevenson et al. (2012) results. The marginalized gas posteriors (Figure 3) show an upper limit on methane, a strong peak in the probability distribution for water near $\sim 10^{-5}$ with an unconstrained tail towards low abundances, and a preference for large ($> 10^{-4}$) abundances of CO. These results are consistent with the planet's relatively high atmospheric temperature (∼1700 K), which tends to favor CO over CH_4 at near-solar abundances. There is a slight preference for high abundances of CO_2 (relative to solar) consistent with the Stevenson et al. (2012) results. We find a C to O ratio that is consistent with solar and can rule out ratios greater than unity. Our temperature profiles are most consistent with the solar metallicity model from Stevenson et al. (2012) without an inversion. Our range of temperature profiles are also similar to those in Fortney et al. (2006) over the IR photosphere. We are in good agrement with their general conclusions that this planet lacks a strong dayside temperature inversion.

3.4. *WASP-12b*

The atmosphere of hot Jupiter, WASP-12b has generated some excitement as the first candidate for a planet with a super-solar C to O ratio. Madhusudhan et al. (2011a) carried out a retrieval analysis and found that their fits preferred a high C/O ratio atmosphere based on seven broadband photometry points ranging from J-band through the Spitzer IRAC 8 micron point. This conclusion stems primarily from the apparent lack of water absorption in the near-infrared. Due to the difficulty in removing water via disequilibrium processes, Madhusudhan et al. (2011a) argue that the most plausible explanation for the low water abundance is a high C to O ratio. Öberg et al. (2011) have suggested that gas giant planets could form with different C to O ratios depending on their location in the protoplanetary disk, suggesting that C to O ratios for hot Jupiters could provide constraints on their formation locations.

Since the publication of the Madhusudhan et al. (2011a) analysis there have also been some corrections to the estimated secondary eclipse depths for this planet. Bergfors et al. (2013) identified a companion star to WASP-12 responsible for contaminating the measured photometry. Crossfield et al. (2012) reanalyzed the Spitzer data to account for contamination from the binary M star companion (Bechter et al. 2013), which dilutes the light from the primary star and decreases the measured eclipse depths. The same paper also presents new K band measurements along with the HST WFC3 data from Swain et al. (2013). Their updated data-model comparison indicates that a nearly isothermal atmosphere without the presence of significant absorbers could explain the data. Swain et al. (2013) observed WASP-12b in both emission and transmission using the HST WFC3. Like Crossfield et al. (2012), they also find that the data do not require a high C to O ratio, particularly if metal oxides are included to explain the transmission spectrum.

Our DEMC retrieval produces two well defined modes. One mode results in an inversion-free atmosphere while the second mode results in a nearly isothermal atmosphere with a weak inversion and a high mixing ratio of CO_2 ($> 10\%$). We exclude this second mode when calculating the retrieval statistics, although we present a representative spectrum and temperature profile of the second mode in Figures 1 and 2, respectively. The 68% confidence interval from our results overlaps with those abundances found in Madhusudhan et al. (2011a) and Swain et al. (2013), although our derived overall abundances are less than those in Madhusudhan et al. (2011a). This discrepancy may be due to our use of the updated secondary eclipse values from Crossfield et al. (2012), which take into account contamination from the binary M star companion, and include the Cowan et al. (2012) 3.6 and 4.5 μm Spitzer photometry as well as the Swain et al. (2013) WFC3 data, although see Madhusudhan (2012) . Our retrieved abundances favor C to O ratios less then much more so than C to O ratios larger than one. Figure 4 demonstrates that the data significantly improve our knowledge over the prior as the long wings in the C/O are ruled out. The C/O ratio we find is still higher than the one reported in Swain et al. (2013). This is likely because we have not include metal oxides in our model, which in any abundance would tend to reduce the overall C/O. If we include the second mode with a large CO_2 abundance then the C to O ratio is closer to 0.5, as the large CO_2 fraction dominates the calculation of this quantity.

These observations also provide strong constraints on the temperature in the deep (100 mbars to 5 bars) atmosphere. This is because the wavelengths probed by the WFC3 data have deep thermal emission weighting functions due to the the lack of significant water opacity. Our retrieved temperature profile is, on average, a few hundred K hotter than the suite of profiles derived in Madhusudhan et al. (2011a), although the general structure is the same. Our fits prefer a highly constrained isothermal region extending up to 100 mbars which then decreases monotonically at lower pressures. We also find that the temperatures at all levels are in the regime where TiO should be in the gas phase. Hence, one would expect an inversion to persist, if TiO is indeed the absorber responsible for the formation of the temperature inversions. Our observations appear to rule out the presence of a strong inversion in WASP-12b's atmosphere. Madhusudhan et al. (2012) have suggested that an enhanced C to O ratio could explain the lack of a TiO-induced temperature inversion in this planet's atmosphere. As mentioned above, our new fits appear to be inconsistent with C to O ratios larger than one, suggesting that this hypothesis is unlikely to be the correct explanation for WASP-12b's missing inversion. We discuss this further in §4

3.5. *WASP-19b*

Given its high equilibrium temperature (2400 K) and the assumption of solar elemental abundances, WASP-19b is expected to have moderate quantities of TiO and VO, hence causing a thermal inversion (Fortney et al. 2008). Anderson et al. (2013) and Madhusudhan (2012) found no evidence for an inversion, leading Madhusudhan (2012) to suggest a high C to O ratio in order to deplete TiO and VO. WASP-19 is one of the most active stars to host a hot Jupiter, therefore UV destruction of an absorbing molecule could also provide an alternative explanation (e.g. Knutson et al. 2010). Madhusudhan (2012) explored both carbon-rich and oxygen-rich models for this planet and concluded that the observations are unable to constrain the C to O ratio, but may slightly favor a C to O ratio greater than one.

Figure 3 suggests that CO and methane are almost completely unconstrained, as their marginalized posteriors closely track the prior. The data do appear to place an upper limit on water ($\sim 10^{-3}$) and a weak upper limit on CO_2 ($\sim 10^{-2}$). We concur with Madhusudhan (2012), who conclude that the current data for this planet do not provide useful constraints on the C to O ratio (Figure 4). Both the oxygen rich and carbon rich derived abundances of Madhusudhan (2012) are consistent with our 68% confidence intervals as well as the temperature profiles. Future observations of WASP-19b with WFC3 would greatly reduce the uncertainties in the gas abundances and temperature profile. Figure 1 shows a large divergence in the spectra at wavelengths less than 2 μm. WFC3 observations with a signal to noise similar to those obtained for WASP-12b would narrow this dispersion down and ultimately reduce the uncertainties in the abundance of H_2O. A strong lower bound on the

water abundance would provide improved constraints on the C to O ratio.

3.6. *WASP-43b*

WASP-43b has a very favorable planet-star radius ratio and correspondingly deep secondary eclipses, making it a prime target for both ground and space-based observations. It is currently one of the coolest (∼1500 K) planets accessible via ground based observations. Blecic et al. (2013) explored the composition of WASP-43b using the temperature and abundance retrieval approach of Madhusudhan et al. (2011a). They found that the composition is only weakly constrained, but rule out a temperature inversion based on the relative fluxes between the Spitzer IRAC channels and the ground based J and K band photometry. We obtain stronger constraints from our fits that allow us to confidently rule out C to O ratios larger than one (Figure 4). This is primarily due to the upper limit on methane near $\sim 10^{-5}$ (Figure 3). We also find that the temperature profile lacks a temperature inversion, consistent with the conclusions of Blecic et al. (2013).

3.7. *TrES-2b*

TrES-2b is a highly irradiated hot-Jupiter that is theoretically predicted to possess a temperature inversion (a "pM" class planet, Fortney et al. 2008). Croll et al. (2010a) compared the spectral energy distribution of photometric data points at 2.14, 3.6, 4.5, 5.6, and 7.8 μm to forward models of Fortney et al. (2005; 2006; 2008) which assume local thermal equilibrium and solar metallicity. Depending on the details of the temperature profile, TiO could be present in gas phase, leading to the formation of a temperature inversion in TrES-2b's atmopshere. They found that cooler temperature profiles fit the data better, naturally explaining the absence of an inversion as TiO and VO should condense out of the planet's dayside atmosphere.

We find that in our fits the data provide minimal constraints on the relative molecular abundances. The marginalized posterior distributions show very little preference for a specific combination of abundances (i.e., there is no strong mode, Figure 3). Although we quote a 68% confidence interval for each species, we note that these confidence intervals are nearly the same as those given by the prior, suggesting relatively weak constraints from the data aside from a slight preference for higher abundances of methane. As a result of these weak constraints, we cannot make strong statements about the C to O ratio. Our retrievals rule out a thermal inversion, in agreement with the results from Croll et al. (2010a). We find that the dispersion in the temperature profiles straddles the TiO condensation boundary, with temperatures between 300 mbars and 0.7 mbars dipping below the condensation temperatures. This suggests that TiO and VO would likely be lost to cold traps in these cooler regions even if there are local regions in the atmopshere that are warm enough for them to exist in gas phase (e.g., Spiegel et al. 2009; Showman et al. 2009).

3.8. *TrES-3b*

Like TrES-2b, TrES-3b is an interesting target for identifying thermal inversions that may be due to TiO (Fortney et al. 2008). Croll et al. (2010b) examined H and K band photometry combined with Spitzer photometry in order to determine the temperature structure. They found that the atmosphere could be explained with an isothermal temperature structure. Our retrievals allow us to expand on these initial conclusions, which were based on a comparison to the same class of forward models by Fortney et al. cited in the previous discussion on TrES-2b. We find that H_2O is fairly well constrained with abundances near 10^{-4}. This is reasonable for a planet at these temperatures with solar composition. Methane has a well defined upper limit of $\sim 10^{-6}$, again consistent with solar composition. CO remains unconstrained due to the large uncertainty on the IRAC 4.5 μm data point and the lack of constraints from data at other wavelengths (Figure 3). CO_2 has a weak upper limit near 10^{-4}. This upper limit arrises from the wings of the 2.1 μm CO_2 band probed by the K band photometry. These abundances are generally consistent with a solar composition atmosphere. We can also confidently rule out C/O ratios larger than one due to the well constrained water abundance and low upper limit to the methane abundance. The temperature profile dispersion for TrES-3b is largely cooler than those of TrES-2b over the range of pressures probed by these infrared observations, and lies well below the condensation curve for TiO. The lack of inversions in TrES-2 and -3b therefore appears to be consistent with the hypothesis that TiO and VO could be the inversion-causing opacity sources.

4. DISCUSSION & CONCLUSIONS

Secondary eclipse spectra simultaneously tell us about the dayside temperature structures and compositions of the planets examined in our study. We have performed a comprehensive, uniform retrieval analysis of eight exoplanets observed in secondary eclipse and provide a catalogue of the resulting temperature and molecular abundance estimates. Such analyses provide a useful set of atmospheric information that can be used to test various hypotheses about the origin of the observed properties of hot Jupiter atmospheres. Our results are generally consistent with those of previous investigations despite differences in model assumptions and retrieval approaches. However, unlike previous investigations, we find no compelling evidence in support of C to O ratios larger than unity as shown in Figure 4. We also find no evidence for thermal inversions in the planets we investigated. Out of our sample of eight planets, two (WASP-19b, WASP-12b) are hot enough to contain TiO in the gas phase, but our retrievals do not detect inversions in their atmospheres. Madhusudhan (2012) have suggested that high C to O ratios could reduce the gas phase TiO and VO abundances. However, we find little evidence in support of high C to O ratios for these two planets, although we cannot rule out high C to O ratios in WASP-19b. This would seem to provide another line of evidence against TiO and VO as the absorber responsible for the inversions, although it does not rule out the more general hypothesis that variations in elemental abundances are responsible for the lack of temperature inversions in a subset of hot Jupiters.

In the future, spectroscopic observations of these planets with the HST WFC3 instrument offer a promising avenue for further constraining their C to O ratios and refining our knowledge of their atmospheres. As can

be seen in Figure 1, WASP-19b, WASP-43b, TrES-2b, and TrES-3b all have widely divergent spectra between 1 and 2 μm. Comparing these spectral spreads to that for WASP-12b, we find that the WFC3 data reduces the overall uncertainty in the retrieved parameters. The WFC3 data acts as a strong baseline for constraining the temperatures in the deep atmosphere. If comparable signal-to-noise could be obtained for the other planets using WFC3, we could expect similar retrieved temperature precisions. WFC3 measurements of HD189733b during secondary eclipse would also help to confirm or refute the high CO_2 abundance required to explain the NICMOS data. In the longer term, higher resolution, high signal-to-noise instruments such as those planned for the James Webb Space Telescope will enable definitive determinations of the atmospheric properties of hot Jupiters.

5. ACKNOWLEDGEMENTS

We thank Jonathan Fortney for insightful conversations. This research was supported in part by an NAI Virtual Planetary Laboratory grant from the University of Washington to the Jet Propulsion Laboratory and California Institute of Technology.

REFERENCES

Allard, F., Hauschildt, P. H., & Schweitzer, A. 2000, ApJ, 539, 366
Anderson, D. R., Smith, A. M. S., Madhusudhan, N., et al. 2013, MNRAS, 430, 3422
Bechter, E. B., Crepp, J. R., Ngo, H., et al. 2013, arXiv:1307.6857
Benneke, B., & Seager, S. 2012, ApJ, 753, 100
Bergfors, C., Brandner, W., Daemgen, S., et al. 2013, MNRAS, 428, 182
Blecic, J., Harrington, J., Madhusudhan, N., et al. 2013, arXiv:1302.7003
Charbonneau, D., Knutson, H. A., Barman, T., et al. 2008, ApJ, 686, 1341
Cowan, N. B., Machalek, P., Croll, B., et al. 2012, ApJ, 747, 82
Crossfield, I. J. M., Barman, T., Hansen, B. M. S., Tanaka, I., & Kodama, T. 2012, ApJ, 760, 140
Croll, B., Albert, L., Lafreniere, D., Jayawardhana, R., & Fortney, J. J. 2010a, ApJ, 717, 1084
Croll, B., Jayawardhana, R., Fortney, J. J., Lafrenière, D., & Albert, L. 2010b, ApJ, 718, 920
Ford, E. B. 2005, AJ, 129, 1706
Fortney, J. J., Marley, M. S., Lodders, K., Saumon, D., & Freedman, R. 2005, ApJ, 627, L69
Fortney, J. J., Saumon, D., Marley, M. S., Lodders, K., & Freedman, R. S. 2006, ApJ, 642, 495
Fortney, J. J., Lodders, K., Marley, M. S., & Freedman, R. S. 2008, ApJ, 678, 1419
Grillmair, C. J., Charbonneau, D., Burrows, A., et al. 2007, ApJ, 658, L115
Grillmair, C. J., Burrows, A., Charbonneau, D., et al. 2008, Nature, 456, 767
Guillot, T. 2010, A&A, 520, A27
Hebb, L., Collier-Cameron, A., Loeillet, B., et al. 2009, ApJ, 693, 1920
Hellier, C., Anderson, D. R., Collier-Cameron, A., et al. 201a, ApJ, 730, L31
Hellier, C., Anderson, D. R., Collier Cameron, A., et al. 2011b, A&A, 535, L7
Heng, K., Hayek, W., Pont, F., & Sing, D. K. 2012, MNRAS, 420, 20
Hubeny, I., Burrows, A., & Sudarsky, D. 2003, ApJ, 594, 1011
Knutson, H. A., et al. 2009, ApJ, 690, 822
Knutson, H. A., Howard, A. W., & Isaacson, H. 2010, ApJ, 720, 1569
Lee, J.-M., Fletcher, L. N., & Irwin, P. G. J. 2012, MNRAS, 420, 170
Line, M. R., Liang, M. C., & Yung, Y. L. 2010, ApJ, 717, 496
Line, M. R., Vasisht, G., Chen, P., Angerhausen, D., & Yung, Y. L. 2011a, ApJ, 738, 32
Line, M. R., Zhang, X., Vasisht, G., et al. 2012, ApJ, 749, 93
Line, M. R., Wolf, A. S., Zhang, X., et al. 2013, ApJ, 775, 137
Madhusudhan, N., & Seager, S. 2009, ApJ, 707, 24
Madhusudhan, N., & Seager, S. 2009, ApJ, 707, 24
Madhusudhan, N., Harrington, J., Stevenson, K. B., et al. 2011a, Nature, 469, 64
Madhusudhan, N., & Seager, S. 2011, ApJ, 729, 41
Madhusudhan, N., Mousis, O., Johnson, T. V., & Lunine, J. I. 2011b, ApJ, 743, 191
Madhusudhan, N. 2012, ApJ, 758, 36
Miller-Ricci Kempton, E., Zahnle, K., & Fortney, J. J. 2012, ApJ, 745, 3
Moses, J. I., Visscher, C., Fortney, J. J., et al. 2011, ApJ, 737, 15
Moses, J. I., Madhusudhan, N., Visscher, C., & Freedman, R. S. 2013a, ApJ, 763, 25
Moses, J. I., Line, M. R., Visscher, C., et al. 2013b, arXiv:1306.5178
Öberg, K. I., Murray-Clay, R., & Bergin, E. A. 2011, ApJ, 743, L16
Press, W.H., Teukolksy, S., Vetterling, W.T., Fannery, B. 1995, Numerical Recipies: The artof scientific computing, sec. ed., Camb. Univ. Press
Robinson, T. D., & Catling, D. C. 2012, ApJ, 757, 104
Rodgers, C. D. 1976, Reviews of Geophysics and Space Physics, 14, 609
Rodgers, C.D., Inverse methods for atmospheric sounding, Theory and Practice, 2000
Sato, B., Fischer, D. A., Henry, G. W., et al. 2005, ApJ, 633, 465
Shabram, M., Fortney, J. J., Greene, T. P., & Freedman, R. S. 2011, ApJ, 727, 65
Showman, A. P., Fortney, J. J., Lian, Y., et al. 2009, ApJ, 699, 564
Sozzetti, A., Torres, G., Charbonneau, D., et al. 2009, ApJ, 691, 1145
Spiegel, D. S., Silverio, K., & Burrows, A. 2009, ApJ, 699, 1487
Stevenson, K. B., et al. 2010, Nature, 464, 1161
Stevenson, K. B., Harrington, J., Fortney, J. J., et al. 2012, ApJ, 754, 136
Swain, M. R., Vasisht, G., Tinetti, G., et al. 2009a, ApJ, 690, L114
Swain, M., Deroo, P., Tinetti, G., et al. 2013, Icarus, 225, 432
ter Braak, C. J., & Vrugt, J. A. 2008, Statistics and Computing, 18, 435-446

TABLE 1
Planet and system parameters.

Planet	R_p (R_{Jup})	R_* ($R_\odot$)	T_* (K)	a (A.U.)	log(g_p) (cm s^{-2})	Ref.
HD189733b	1.138	0.756	5040	0.031	3.34	Torres et al. (2008)
GJ436b	0.3767	0.464	3350	0.02872	3.107	Torres et al. (2008)
HD149026b	0.654	1.37	6160	0.04313	3.132	Torres et al. (2008); Carter et al. (2009)
WASP-12b	1.79	1.57	6300	0.0229	3.0	Hebb et al. (2009)
WASP-19b	1.386	0.990	5500	0.01632	3.19	Hebb et al. (2010); Hellier et al. (2011a)
WASP-43b	0.93	0.60	4400	0.0142	3.67	Hellier et al. (2011b)
TrES-2b	1.224	1.003	5850	0.03558	3.298	Torres et al. (2008)
TrES-3b	1.336	0.812	5650	0.023	3.4	Torres et al. (2008); Sozzetti et al. (2009)

TABLE 2
Sources of secondary eclipse data. The wavelengths of the channels are given in microns.

Planet	Spectroscopic Data Sources	Broadband Data Sources
HD189733b	HST NICMOS[a] (Swain et al. 2009), Spitzer IRS[b] (Grillmair et al. 2007)	Spitzer IRAC[c] 3.6, 4.5 (Knutson et al. 2012), 5.7, 7.8 (Agol et al. 2010)
GJ436b	-	Spitzer IRAC 3.6, 4.5, 5.7, 7.8, IRS 16,MIPS[d] 23 (Stevenson et al. 2010)
HD149026b	-	Spitzer IRAC 3.6, 4.5, 5.7, 7.8, IRS 16 (Stevenson et al. 2012)
WASP-12b	HST WFC3[f] (Swain et al. 2013)	CFHT WIC 1.66, 2.15 (Croll et al. 2011), Spitzer IRAC 3.6, 4.5, 5.7, 7.8 (Crossfield et al. 2012)
WASP-19b	-	VLT HAWK-I[g]1.620 (Anderson et al. 2010), 2.095 (Gibson et al. 2010), Spitzer IRAC 3.6, 4.5, 5.7, 7.8 (Anderson et al. 2013)
WAS43b	-	VLT HAWK-I 1.19, 2.1 (Gillon et al. 2012), Spitzer IRAC 3.6, 4.5 (Blecic et al. 2013)
TrES-2b	-	CFHT WIC[e] 2.15 (Croll et al. 2010a), Spitzer IRAC 3.6, 4.5, 5.7, 7.8 (O'Donovan et al. 2010)
TrES-3b	-	CFHT WIC 2.15 (Croll et al. 2010b), Spitzer IRAC 3.6, 4.5, 5.7, 7.8 (Fressin et al. 2010)

[a] Hubble Space Telescope Near Infrared Camera and Multi-Object Spectrometer
[b] Infrared Spectrometer
[c] nfrared Array Camera
[d] Multiband Imaging Photometer for Spitzer
[e] Canada-France-Hawaii Telescope Wide-field Infrared Camera
[f] Wide Field Camera 3
[g] Very Large Telescope High Acuity Wide field K-band Imager

TABLE 3
Summary of the abundance retrieval results for each planet compared with the literature.[a]

Planet	Source	H_2O[b]	CH_4[b]	CO[b]	CO_2[b]	C/O[c]
HD189733b	Best Fit (χ^2_{best}/N =2.27)	8.86×10^{-4}	19.8×10^{-6}	182×10^{-4}	2.87×10^{-3}	0.85
	68% Interval	$[3.38 - 12.8] \times 10^{-4}$	$[9.97 - 23.9] \times 10^{-6}$	$[0.275 - 307] \times 10^{-4}$	$[1.29 - 3.73] \times 10^{-3}$	0.47 - 0.90
	Madhusudhan & Seager 2009	$[0.1 - 10] \times 10^{-4}$	$<$few$\times 10^{-6}$	$[1 - 100] \times 10^{-4}$	$\sim 70 \times 10^{-3}$	0.007 - 1
	Swain et al. 2009	$[0.1 - 1] \times 10^{-4}$	$< 10 \times 10^{-6}$	$[1 - 3] \times 10^{-4}$	$[0.0001 - 0.001] \times 10^{-3}$	0.5 - 1
	Lee et al. 2012	$[0.3 - 100] \times 10^{-4}$	$< 100 \times 10^{-6}$	-	$[0.15 - 30] \times 10^{-3}$	0.30 - 1
	Line et al. 2012	$[0.5 - 3] \times 10^{-4}$	$< 10000 \times 10^{-6}$	$[36 - 360] \times 10^{-4}$	$[1.7 - 6.7] \times 10^{-3}$	-
GJ436b	Best Fit (χ^2_{best}/N =1.78)	5.56×10^{-6}	5.65×10^{-9}	34.5×10^{-3}	3.18×10^{-7}	1.0
	68% Interval	$[0.00071 - 105] \times 10^{-6}$	$[0.0067 - 24.5] \times 10^{-9}$	$[0.016 - 66.4] \times 10^{-3}$	$[0.0411 - 8720] \times 10^{-7}$	0.50 - 1.0
	Madhusudhan & Seager 2011	$< 100 \times 10^{-6}$	$[100 - 1000] \times 10^{-9}$	$> 1 \times 10^{-3}$	$[10 - 1000] \times 10^{-7}$	0.5 - 1.0
	Stevenson et al. 2010	3×10^{-6}	100×10^{-9}	0.7×10^{-3}	1×10^{-7}	-
HD149026b	Best Fit (χ^2_{best}/N =0.23)	172×10^{-7}	0.032×10^{-10}	21×10^{-6}	19×10^{-7}	0.55
	68% Interval	$[0.0034 - 890] \times 10^{-7}$	$[0.072 - 290] \times 10^{-10}$	$[0.00024 - 11400] \times 10^{-6}$	$[0.0042 - 7170] \times 10^{-7}$	0.45 - 1.0
WASP-12b	Best Fit (χ^2_{best}/N =2.45)	0.15×10^{-8}	1.40×10^{-6}	4.9×10^{-7}	9.39×10^{-6}	0.59
	68% Interval	$[0.00093 - 12] \times 10^{-8}$	$[0.65 - 3.10] \times 10^{-6}$	$[0.0004 - 368] \times 10^{-7}$	$[2.44 - 23] \times 10^{-6}$	0.54 - 0.95
	Madhusudhan et al. 2011	$[0.005 - 600] \times 10^{-8}$	$[4 - 800] \times 10^{-6}$	$[300 - 30000] \times 10^{-7}$	$[0.2 - 7] \times 10^{-6}$	$>$1.0
	Swain et al. 2013	$[0.0080047 - 2000000] \times 10^{-8}$	$[0.09 - 6.12] \times 10^{-6}$	$[0.00011 - 5670000] \times 10^{-7}$	$[0.007 - 2400] \times 10^{-6}$	0.3
WASP-19b	Best Fit (χ^2_{best}/N =0.032)	130×10^{-7}	1.21×10^{-6}	1900×10^{-6}	62×10^{-8}	0.99
	68% Interval	$[0.00046 - 1080] \times 10^{-7}$	$[0.0015 - 3890] \times 10^{-6}$	$[0.00013 - 5110] \times 10^{-6}$	$[0.0053 - 5950] \times 10^{-8}$	0.26 - 6.33
	Madhusudhan 2012[d]	$[1000/20] \times 10^{-7}$	$[0.0006/0.5] \times 10^{-6}$	$[600/500] \times 10^{-6}$	$[0.06/0.001] \times 10^{-7}$	0.4/1.1
WASP-43b	Best Fit (χ^2_{best}/N =0.28)	2.31×10^{-6}	1.54×10^{-6}	437×10^{-5}	71×10^{-7}	1.00
	68% Interval	$[0.0019 - 1390] \times 10^{-6}$	$[0.00044 - 1.49] \times 10^{-6}$	$[0.00024 - 3590] \times 10^{-5}$	$[0.060 - 816] \times 10^{-7}$	0.052-1.00
TrES-2b	Best Fit (χ^2_{best}/N =0.60)	132×10^{-6}	24.6×10^{-6}	22.4×10^{-7}	0.00010×10^{-7}	0.20
	68% Interval	$[0.00013 - 6300] \times 10^{-6}$	$[0.0011 - 6340] \times 10^{-6}$	$[0.00055 - 11300] \times 10^{-7}$	$[0.00035 - 8760] \times 10^{-7}$	0.021-8.25
TrES-3b	Best Fit (χ^2_{best}/N =0.067)	0.90×10^{-4}	50.4×10^{-9}	247×10^{-7}	57×10^{-8}	0.22
	68% Interval	$[0.13 - 12.5] \times 10^{-4}$	$[0.026 - 257] \times 10^{-9}$	$[0.00076 - 22500] \times 10^{-7}$	$[0.0034 - 1880] \times 10^{-8}$	0.0004-0.97

[a] We present the best fit mixing ratios and the resulting C/O ratio along with their 68% confidence intervals. The best fit is defined as the fit that produces the minimum cost function value, χ^2_{best} from equation 1. We quote the reduced cost-fucntion value as the cost function value divided by the number of data points, N.

[b] Since we place upper and lower limits on the DEMC prior, these results must be interpreted in the context of the prior. The 68% confidence interval resulting from the flat priors alone would give values that range from $8.15 \times 10^{-11} - 1.51 \times 10^{-2}$, or $\sim$8 orders of magnitude. One should use caution when interpreting uncertainties that approach these levels, which is indicative of little information gain from the data.

[c] The C/O ratios resulting from the prior would span $0.051 - 14.5$, or $\sim$ 3 orders of magnitude.

[d] We show both the oxygen rich planet (ORP) values and the carbon rich planet (CRP) values quoted in his investigation [ORP/CRP]

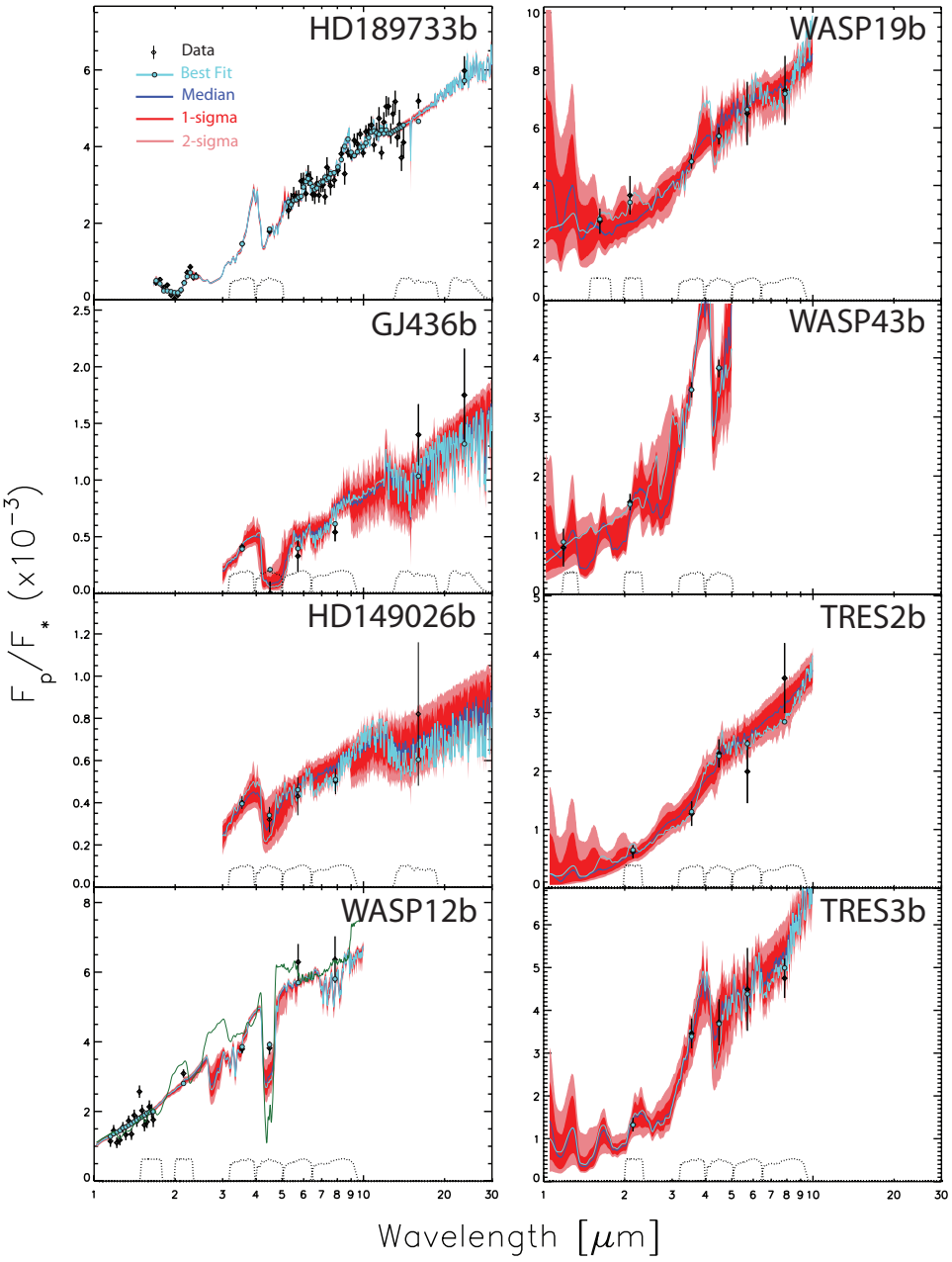

FIG. 1.— Secondary eclipse spectra and fits for each planet resulting from the differential evolution Markov chain Monte Carlo retrieval approach. The diamonds with error bars are the data from the sources in Table 2. The DEMC retrievals produce several hundred thousand spectra. The best fit of this ensemble is shown in light blue. The light blue circles are the best fit model binned to the data. The ensemble of spectra are summarized with the median spectra (blue) and the 1- and 2-sigma confidence intervals (dark red and light red respectively). The green spectrum in the WASP-12b panel is representative of the second mode (see text). The dotted curves at the bottom of each panel are the filter profiles for each broadband measurement.

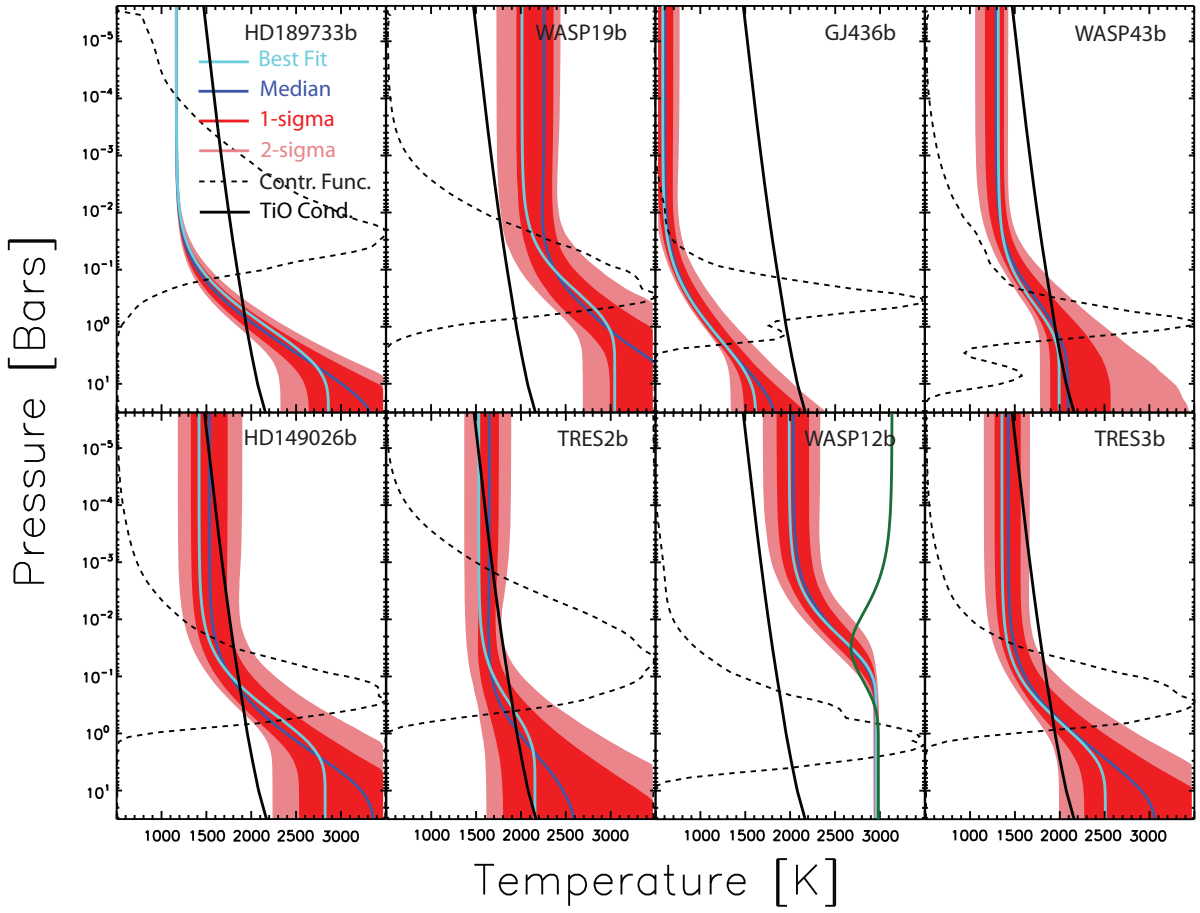

FIG. 2.— Summary of the retrieved temperature profiles. The best fit temperature profile is shown in light blue. The ensemble of temperature profiles are summarized with the 1 (dark red)- and 2 (light red)-sigma confidence intervals and the median of the profiles (dark blue). The dashed curves are the wavelength averaged thermal emission contribution functions. These represent on a whole, where the emission is coming from. The solid black line in each panel is the TiO condensation curves for 1x solar composition (Fortney et al. 2008). The green profile in the WASP-12b panel is representative of the second mode (see text).

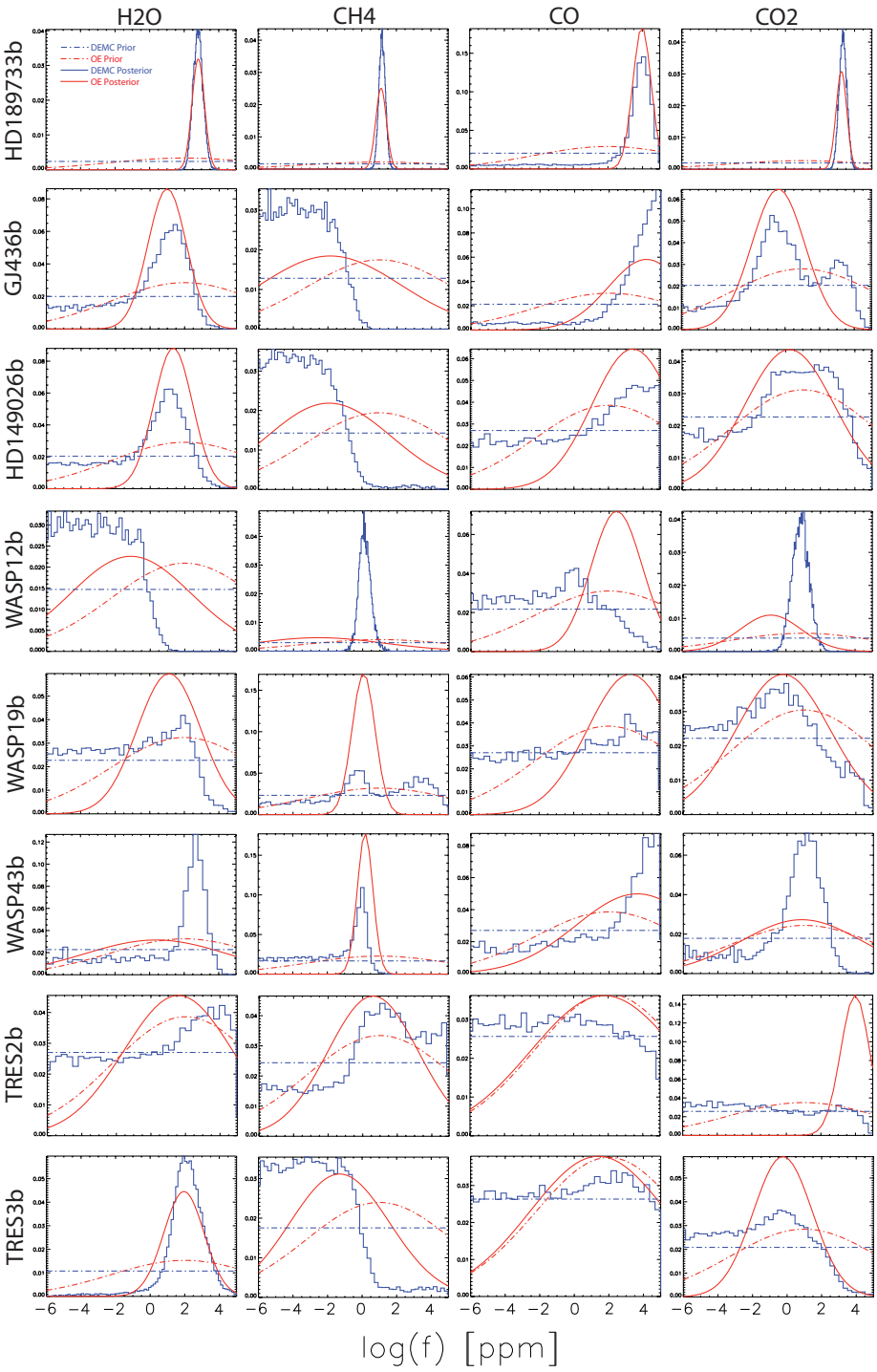

FIG. 3.— Histograms of the marginalized posterior probability distribution for each of the retrieved gases (columns) for each planet (rows). The Gaussian probability distributions derived from the optimal estimation retrievals are shown in red and differential evolution Markov chain Monte Carlo results are in blue. The priors for DEMC and OE are shown as the blue and red dot-dashed curves. The y-axis is the normalized probability density for each gas with arbitrary units.

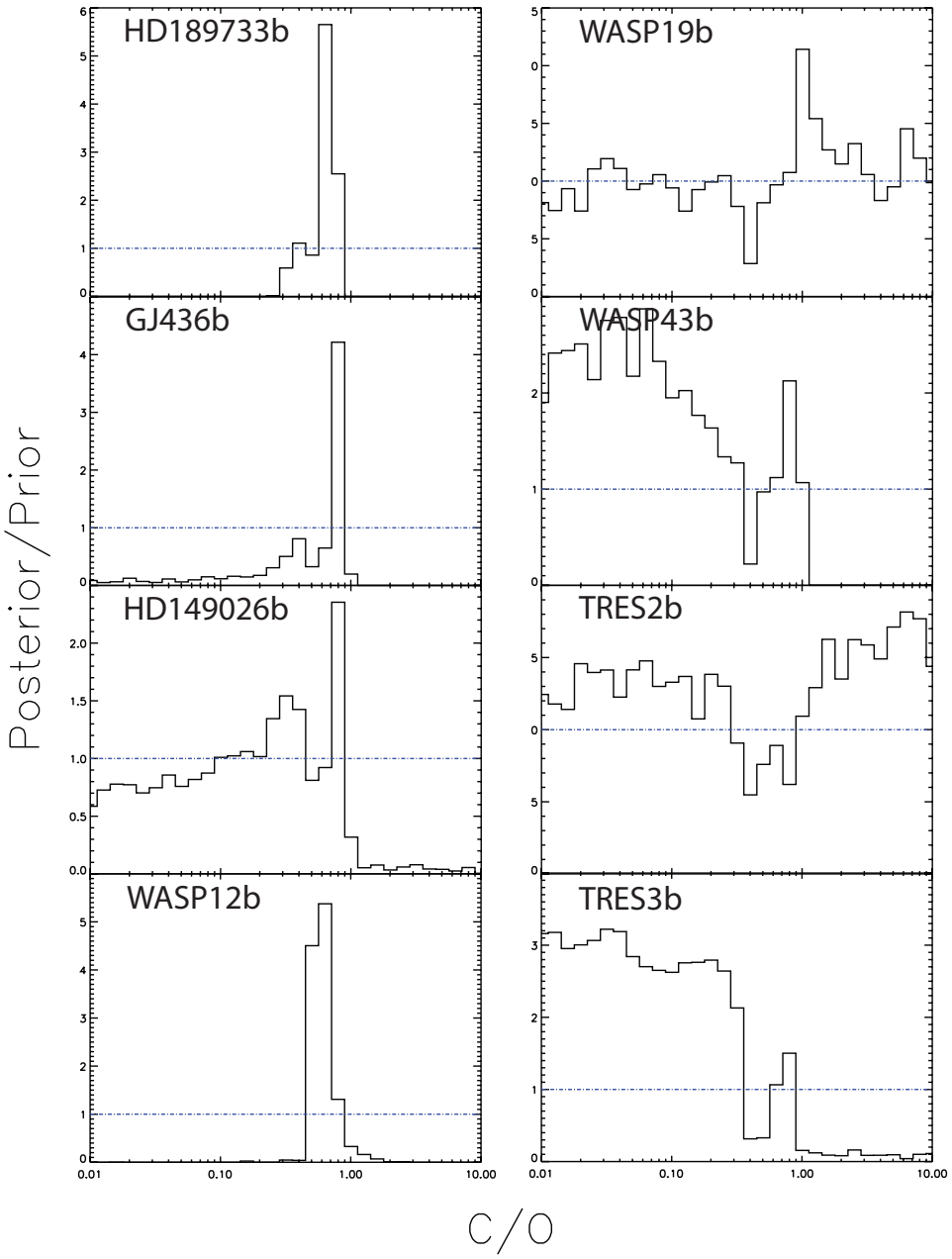

FIG. 4.— Resulting prior-normaized C/O ratio probability distributions for each planet. These distributions are derived by dividing the double peaked prior described in Paper I into the C/O distributions that result from the posterior gas distributions. Although this has no statistical meaning, it is a useful way to visualize how the data contributes to our knowledge of the C/O. The horizontal blue dot-dashed line is the curve resulting from the C/O prior in Part I divided by itself. See §3 for more details.